Nucleation and Phase Selection in Undercooled Melts: Magnetic Alloys of Industrial Relevance (MAGNEPHAS)

Wolfgang LÖSER[1], Regina HERMANN[1], Thomas G. WOODCOCK[1], Jan FRANSAER[2], Mikhail KRIVILYOV [2], László GRÁNÁSY[3], Tamás PUSZTAI[4], Gyula I. TÓTH[4], Dieter M. HERLACH[5], Dirk HOLLAND-MORITZ[5], Matthias KOLBE[5], and Thomas VOLKMANN[5]

[1] Leibniz Institute for Solid State and Materials Research (IFW) Dresden, Germany, loeser@ifw-dresden.de
[2] Katholieke Universiteit Leuven (KUL), Belgium
[3] Brunel Centre for Advanced Solidification Technology, Brunel University, West London, UK
[4] Research Institute for Solid State Physics and Optics, Budapest, Hungary
[5] Institut für Materialphysik im Weltraum, Deutsches Zentrum für Luft- und Raumfahrt (DLR), D-51170 Köln, Germany

Abstract

Studies of phase selection and microstructure evolution in high-performance magnetic materials are an urgent need for optimization of production routes. Containerless solidification experiments by electromagnetic levitation and drop tube solidification were conducted in undercooled melts of Fe-Co, Fe-Ni soft magnetic, and Nd-Fe-B hard magnetic alloys. Melt undercooling under microgravity was achieved in the TEMPUS facility during parabolic flight campaigns. For Fe-Co and Fe-Ni alloys significant effects of microgravity on metastable phase formation were discovered. Microstructure modifications as well as metastable phase formation as function of undercooling and melt flow were elucidated in Nd-Fe-B. Modeling of solidification processes, fluid flow and heat transfer provide predictive tools for microstructure engineering from the melt. They were developed as a link between undercooling experiments under terrestrial and microgravity conditions and the production routes of magnetic materials.

1. Introduction

Optimization of production routes and development of novel high-performance hard and soft magnetic materials require accurate knowledge of phase selection and microstructure evolution processes. Containerless solidification by electromagnetic levitation (EML) and drop tube processing (DTP) are applied for revealing metastable phase formation in Fe-Co, Fe-Ni and Nd-Fe-B undercooled melts. Melt undercooling experiments were performed on ground-based EML equipment and temperature-time profiles were recorded from a high-speed photo diode. Undercooling experiments under microgravity conditions were carried out during parabolic flight campaigns with the TEMPUS facility. The installation of a high-speed camera in the advanced TEMPUS equipment permits recording of the solidification front in undercooled melts.

Modeling of solidification, fluid flow and heat transfer provide predictive tools for microstructure engineering from the melt. They were developed as a link between undercooling experiments under terrestrial and microgravity conditions and the production routes of magnetic materials.

2. Fe-Co and Fe-Ni Soft Magnetic Alloys

Commercial alloys based on Fe-Co and Fe-Ni are widely used soft magnetic materials. Fe-Co alloys with > 18 at.% Co and Fe-Ni alloys with > 5 at.% Ni display the γ-Fe (*fcc*) primary phase in conventional solidification processes. Fe-Ni alloys, similar to Fe-Co, can form the metastable phase δ-Fe (*bcc*) if the melt undercooling exceeds a critical level $\Delta T > \Delta T_c$ [1-2]. This is evidenced by a double-recalescence process of temperature-time profiles in EML experiments (**Fig. 1**).

EML experiments during parabolic flights have shown that in microgravity conditions ΔT_c is reduced and the arrest time before the transformation to theequilibrium phase is prolonged due to reduced convection[1,3].

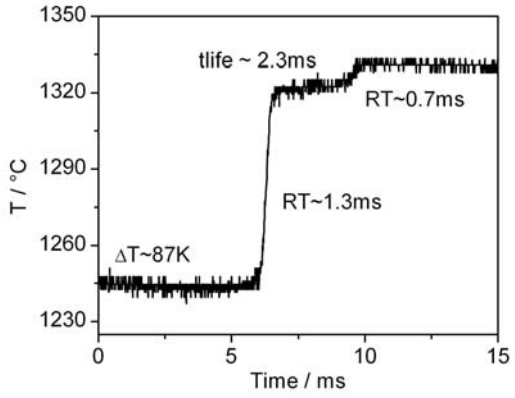

Fig. 1 Temperature time plot of a high-speed photo diode from a parabolic flight experiment with a $Fe_{90}Ni_{10}$ droplet undercooled 87 K showing the double-recalescence with intermediate metastable phase (RT = recalescence time).

For a $Fe_{90}Ni_{10}$ alloy the lifetime of the metastable phase increases from $t_{life} \approx 0.4$ to 1.5 ms (depending on ΔT) on ground to $t_{life} \approx 2.3$ ms (ΔT = 87 K) under microgravity conditions (Fig. 1).

Analyzing the temperature of the thermal arrest during recalescence allows experimental determination of the metastable liquidus and solidus lines. These data can be used to fit calculated metastable phase boundaries, generated by thermodynamic modeling, in order to improve the accuracy of the calculated phase diagram[4] (**Fig. 2**).

The solidification front was observed by high-speed camera in parabolic flight experiments.

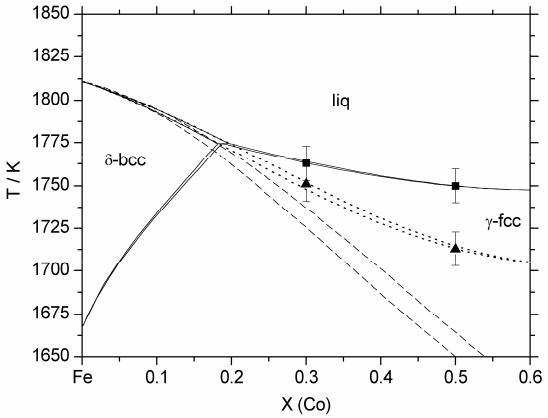

Fig. 2 Fe-Co equilibrium (solid lines) and metastable (dotted lines) phase diagrams calculated using the adjusted database[4]. Experimentally measured equilibrium (squares) and metastable (triangles) solidus tempera tures are also plotted. The metastable phase diagram from the original database is shown for comparison (dashed lines).

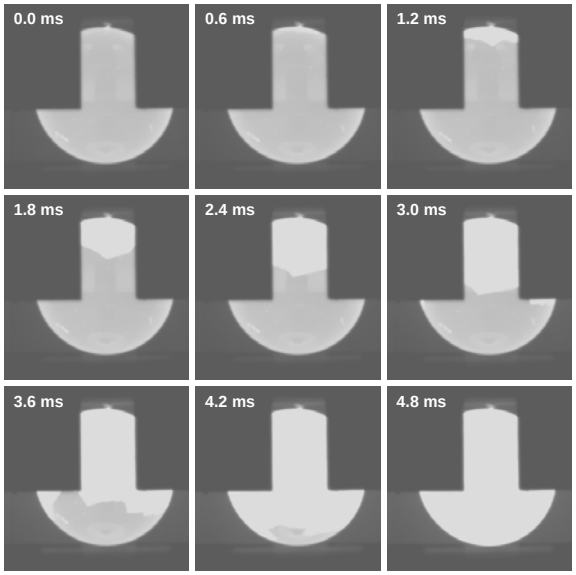

Fig. 3 Picture series from the high speed camera of parabolic flight experiments for $Fe_{90}Ni_{10}$. From the moving front of the solid (bright) into the 72 K undercooled melt (dark) the solidification velocity was evaluated.

A solidification front velocity of v = 1.6 ms^{-1} for a $Fe_{90}Ni_{10}$ sample at ΔT = 72 K undercooling has been evaluated from the space resolved interface (**Fig. 3**), which nicely fits to previous data with the photodiode. This can lead to better understanding of the growth kinetics in undercooled melts but requires modeling of the solidification front geometry.

3. Phase Field Modeling of Nucleation and Phase Selection in the Fe-Ni System

The magnetic properties depend on the crystalline phase and microstructure. It is, thus, of high importance to understand phase selection during solidification. Usually, it happens in the nucleation stage, therefore, a detailed knowledge on possible nucleation pathways is essential. Microscopic theory predicts that in simple liquids, small amplitude fluctuations prefer the *bcc* structure, i.e., nucleation of the *bcc* phase is expected[5]. Indeed, molecular dynamics simulations show that in the Lennard-Jones system, where the *fcc* is the stable phase, the small crystal-like fluctuations have a *bcc* structure, while the larger ones have an *fcc* core surrounded by a *bcc*-like layer[6]. A similar phenomenon is expected in metallic systems. The phase field theory is a powerful tool for investigating both nucleation and crystal growth[7]. Here, we address phase selection in the Fe-Ni system by phase field modeling.

Two types of phase field models will be used in this study. One of them that we call the $\phi - \psi$ *model*, relies on four fields: the phase field ϕ that monitors the solid-liquid transition; a solid-solid order parameter ψ that distinguishes the *fcc* and *bcc* phases; the orientation field, θ that captures the crystallographic orientation of the individual crystallites; and the chemical composition field c. The free energy is a functional of these fields:

$$F = \int dV \left\{ f(\phi,\psi,\theta,c) + \frac{\varepsilon_\phi^2 T}{2}(\nabla\phi)^2 + \frac{\varepsilon_\psi^2(\phi) T}{2}(\nabla\psi)^2 \right\}, \quad (1)$$

where f is the free energy density of the homogeneous system, while square gradient terms are introduced to penalize the spatial variation of ϕ and ψ. The latter give rise to the interfacial/phase boundary energies. As in Ref.[8], we have incorporated a free energy term that ensures a fixed orientation relationship between the crystalline phases at the phase boundaries. All fields are assumed to follow relaxation dynamics with mobilities related to the translational, rotational and chemical diffusion coefficients.

The other type of phase field model, we apply here is the *multi-phase field model* that applies separate phase-field variables for all the crystalline phases and the liquid. The respective free energy functional is sought in the form specified in[9]

$$F = \int dV \left\{ f(\{\phi_i\}) + \sum_{j>i} \frac{\varepsilon_{ij}^2 T}{2} \left(\phi_i \nabla\phi_j - \phi_j \nabla\phi_i \right)^2 \right\}, \quad (2)$$

where $\phi_1 = \phi\psi$, $\phi_2 = \phi(1 - \psi)$ and $\phi_3 = 1 - \phi$,

$\phi_1 + \phi_2 + \phi_3 = 1$. However, instead of the intuitive free energy used in other studies, we apply a free energy function *f* based on the structure dependent free energies obtained by Ginzburg-Landau expansion some time ago[10]. In the present work, we apply this approach to determine the nucleation pathways in the single component limit. The nuclei represent an extreme of the free energy functional. Assuming a spherical symmetry (reasonable for metals), we solve the respective Euler-Lagrange equation numerically by a relaxation method under boundary conditions that prescribe zero field gradients at the center and unperturbed liquid in the far field. A generalization for the binary case is underway.

In performing the computations, we rely on a CALPHAD type assessment of the free energies[11]. The respective phase diagram of the Fe-Ni system (**Fig. 4**) shows not only where the *fcc* and *bcc* solid solutions are stable, but also gives hints on the metastable phase appearance. To fix the model parameters, a 1 nm thick crystal-liquid interface is taken (in agreement with the atomistic simulations), and the experimental values for the interfacial free energies are used[12]. We assume that γ_{fcc} = (0.55/0.32) γ_{bcc}[13], and that the phase boundary energy is twice of the average solid-liquid interfacial energies.

The solidification of samples after quenching to *T* = 1300 K has been explored as a function of composition

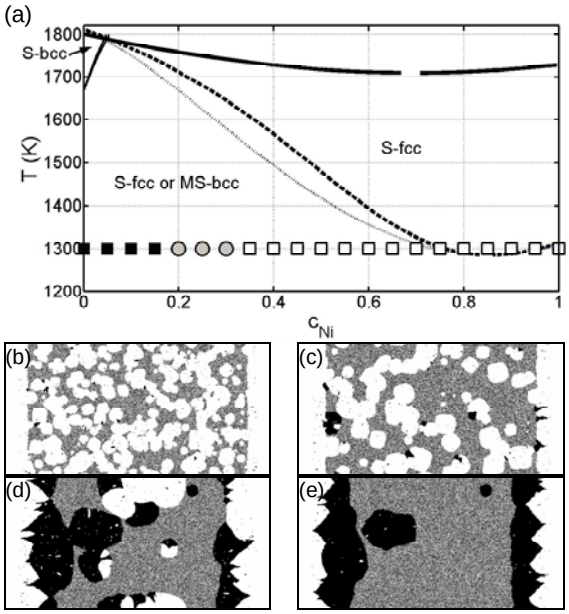

Fig. 4 Phase selection in the Fe-Ni system in the $\phi - \psi$ model. (a) Phase diagram showing the solidus (light) and liquidus (heavy) lines for the *fcc* (solid) and *bcc* (dashed) phases. Black squares, gray circles and empty squares correspond to simulations that resulted in *bcc*, competing *fcc*-*bcc* and *fcc* nucleation, respectively. Panels (b) to (e) show snapshots of the ψ field (white = *bcc*, black = *fcc*) corresponding to simulations with Ni concentrations in the initial liquid of 0.20, 0.25, 0.30 and 0.35, respectively.

within the ϕ–ψ model. The computed microstructures are shown in Figs. 4 (b)-(d). A transition from the nucleation of the stable *fcc* structure on the Ni side to the nucleation of the metastable *bcc* phase on the Fe side has been seen, when decreasing the Ni content of the liquid. Note the relatively broad region, in which *fcc* and *bcc* nucleation compete.

Results for nuclei preferred in pure Fe and Ni as predicted by the multi-phase field model with a structure dependent Ginzburg-Landau free energy are shown in **Fig. 5**. Keeping the thermodynamic driving force constant for the crystal phases stable at the melting point of Fe and Ni (*bcc* and *fcc*, respectively), we observe the appearance of substantially different mixed phase nuclei (see Fig. 5). The respective undercoolings are ΔT_{Fe}^{bcc} = 260 K and ΔT_{Ni}^{fcc} = 150 K. Although in Fe at this undercooling the *fcc* is the stable phase (we are below the *fcc*-*bcc* coexistence) and the driving force for the *fcc* phase is almost as large as for the *bcc* phase, we have a dominantly *bcc* nucleus. Conversely, in the case of Ni (where at the applied undercooling, the *fcc* is stable), there is a considerable *bcc* fraction in the interface, even if temperature is significantly higher than the melting point of the *bcc* phase.

4. Nd-Fe-B Hard Magnetic Alloys

Of vital interest in near-stoichiometric Nd-Fe-B alloys is the suppression of α-Fe, which deteriorates the coercivity. Systematic EML experiments on undercooling Nd-Fe-B melts have been carried out, which proved the competition of Φ-$Nd_2Fe_{14}B$ and γ-Fe solidification as well as the occurrence of a metastable phase χ-$Nd_2Fe_{17}B_x$, x~1 (**Fig. 6**).

However, crystallization of γ-Fe cannot be avoided completely that is explained by multiple nucleation of stable and metastable phases in the undercooled melt [14-15]. In view of application aspects it is of interest to

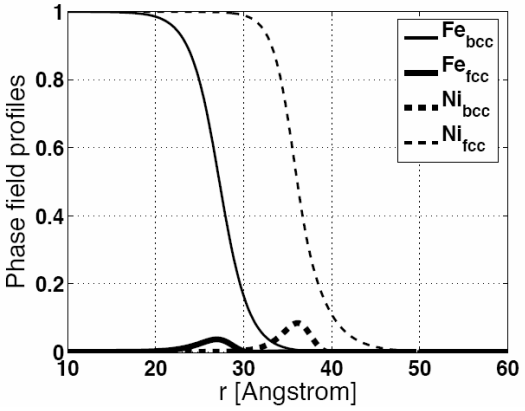

Fig. 5 Phase field profiles of multi-phase field model for pure *Fe* (solid lines) and *Ni* (dashed lines) at the same driving force Δg = −1500 J/mol. Thin and thick lines show the profiles for stable and metastable phases, respectively.

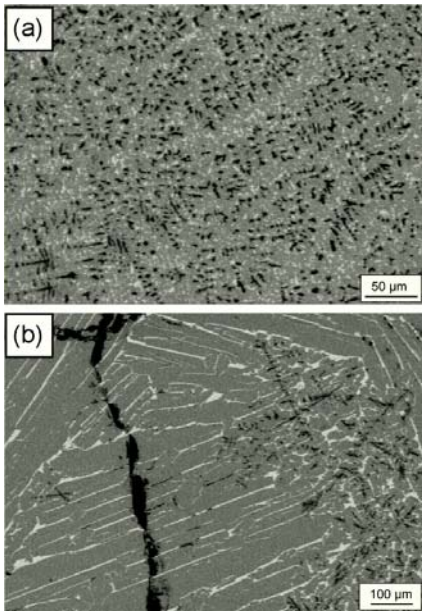

Fig. 6 Scanning electron micrographs in the backscattered mode of undercooled and solidified $Nd_{14}Fe_{79}B_7$ alloys for solidification at temperatures below the peritectic temperature (a) primary solidification of γ-Fe and subsequent formation of the ϕ-phase and (b) sin gle-step solidification of γ+ϕ. The phases in the mi crograph are: α-Fe (black), ϕ-phase (grey), and Nd-rich phase (white).

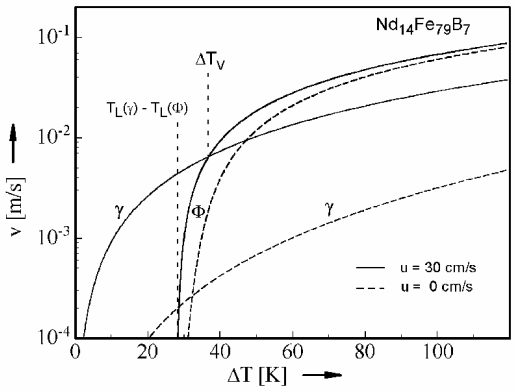

Fig. 7 Calculated dendrite growth velocities of γ-Fe and ϕ-phase as a function of undercooling ΔT in $Nd_{14}Fe_{79}B_7$ alloy melts: with a fluid flow speed of u = 30 cm/s (solid lines) and without convection u = 0 (dashed lines). The critical undercooling ΔT_v marks the transition of preferred growth from the γ-Fe-phase to the ϕ-phase for u = 30 cm/s that is estimated for ground-based EML experiments.

elucidate the mechanism responsible for the suppression of solidification of the γ-Fe-phase as well as the effect of alloying elements on phase formation. A lower flow velocity in the melt, expected under microgravity conditions, can favor the growth of the Φ-phase (**Fig. 7**).

The aim of microgravity experiments were growth velocity measurements of the γ-Fe and ϕ-phases under reduced melt convection and microstructure analyzes of retrieved samples in order to verify predictions of dendrite growth models. However, short-term microgravity experiments with Nd-Fe-B during parabolic flights were not suitable for several reasons. So drop tube experiments were done in helium at ambient temperature and a pressure of 500 mbar.

Rapid solidification of the near-stoichiometric $Nd_2Fe_{14}B$ alloy in DTP was also studied theoretically. In contrast with EML[14], DTP provides much higher cooling rates but interpretation of the experimental data is more difficult as temperature-time profiles cannot be measured and direct observation of the solidification front is impossible. Hence numerical modeling is used in this work to better understand the solidification and phase selection in atomized drops. The main scientific objective of this study was the investigation of the effects of fluid flow and heat transfer on nucleation and phase selection in undercooled melts. The developed models were applied for analysis of the solidification conditions in the Nd-Fe-B alloy in order to increase the amount of Φ phase in the solidified drops. Modeling of drop trajectories in the drop tube, fluid flow, heat transfer, competitive nucleation and growth of different phases inside solidifying droplets was performed (**Fig. 8**). The influence of different processing parameters was studied for drops of 50 - 1000 µm in diameter injected with a velocity of 1 - 5 m/s.

The Bond number calculated at the present experimental conditions is between 0.001 and 0.15, hence the effect of the surface tension (σ=1.8 J/m^2) is large and the drops remain spherical. It was found that small drops achieve their steady velocity quickly after injection while large drops never attain their steady velocity in

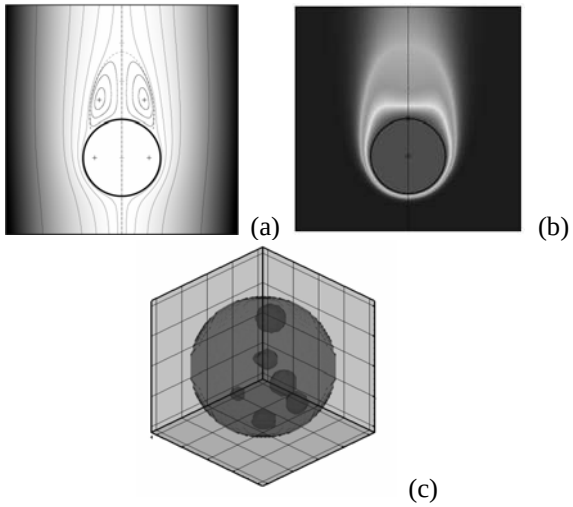

Fig. 8 (a) Fluid flow in terms of the stream function calcu lated at a Reynolds number of 100. (b) Temperature field around an impulsively injected drop. (c) 3D dis tribution of Φ phase nuclei observed at high under cooling.

the drop tube. Hence, the transient fluid flow inside droplets is important. This effect is particularly critical for Nd-Fe-B since convection affects the phase selection in this alloy. It was found that there are two stages in development of the internal flow: 1) adjustment to the external flow defined by the injection velocity, 2) acceleration or deceleration of the internal flow forced by the external flow. The duration of the first stage is comparable to the time necessary for complete solidification so the quasi-steady approximation does not give a reliable estimation of the internal flow velocity. Initially, flow develops in a thin boundary layer near the surface of the drop. The internal flow develops gradually and achieves velocities between 0.1 and 10 mm/s calculated at the moment of recalescence in small and large drops respectively[16]. These values are 1-2 orders of magnitude smaller than the velocities estimated from the steady flow approach which does not consider the transient regime. This estimation does not account for the internal circulation induced by melt break-up and drop formation during injection. The modeling showed that the decay time of the initial internal circulation lies between 0.1 and 5 a^2/ν, where a is the drop radius and ν is the kinematic viscosity of the melt. This time is comparable to the cooling time prior to nucleation.

Heat transfer around drops was studied as a function of the drop size, injection velocity, pressure and temperature of the gas in the drop tube. The transient temperature distribution was calculated using the instantaneous flow field. The temperature field is spherical in small drops and elliptical in large drops. The model predicts temperature differences of about 5 - 10 K inside drops which results in enhanced nucleation near the drop surface. The cooling rates were estimated between 10^5 and 800 K/s for small and large drops. These cooling rates are 2 - 3 orders of magnitude higher than those in EML because droplets are substantially smaller and provide non-equilibrium solidification conditions. Control of the cooling rate can be achieved by variation of the drop radius: a decrease of the drop radius by one order of magnitude gives an increase of the cooling rate by 2 - 3 orders. Variation of the gas pressure and temperature gives a change of about 10 - 30%. Increasing the injection velocity does not affect the cooling rate of small drops and has only a minor effect on big drops. Radiation increases the cooling rate of big drops by 1 - 5% but is negligible for small drops.

The solidification selection diagram of the investigated alloy is complex. In the DTP model, nucleation of only two phases (γ-Fe and Φ) was considered and the peritectic reaction L + γ-Fe → Φ was not regarded. Nucleation of each phase was described in terms of the classic nucleation theory:

$$I = I_0 \xi \exp\left(-\frac{\Delta G^*}{k_B T}\right), \quad \Delta G^* = b\frac{\sigma^3}{\Delta G^2} f(\theta), \quad (3)$$

where I is the nucleation rate, I_0 is the kinetic prefactor, ξ is the factor depending on the nucleation mechanism, ΔG^* is the activation energy, b is the form factor, ΔG is the change of the free Gibbs energy, σ is the interfacial energy and $f(\theta)$ is the potential factor. The heterogeneous nucleation rate was calculated with $I_0 = 10^{41}$ m^{-3} s^{-1}, $\xi = 10^{-11}$ and $f(\theta) = 0.01$ and 0.1 for γ-Fe and Φ, respectively. These values were chosen after comparison of the modeling results with experimental data. The stochastic nature of nucleation was introduced by means of Poisson statistics[17]. First, the nucleation probability is calculated based on the local nucleation rate which is a function of temperature and concentration. Then random Poisson variables are generated whose average rate is given by the local nucleation rate. Finally, a new nucleus is formed at the selected time and position if the random variable is smaller than the time step. This approach accounts for spontaneous nucleation in a temperature interval contrary to the deterministic approach which predicts nucleation at a fixed critical undercooling.

The estimation of the free Gibbs and interfacial energies showed that γ-Fe is the primary phase at small undercooling. The metastable Φ phase becomes the primary phase at high undercooling. Our model predicted the number of nuclei and the critical undercooling interval for each phase. The number of γ-Fe nuclei varies between 200…700 depending on the drop radius and nucleation proceeds at undercoolings of 50…80 K. For the primary nucleation of Φ phase, the number of the Φ nuclei varies between 5…50. The undercooling interval for Φ nucleation between 100…120 K is predicted. The nucleation rate of both phases in a 1000 μm drop is shown as a function of time (**Fig. 9**). The nucleation rate of γ-Fe is one order of magnitude bigger than that of Φ. The nucleation period takes about 0.05 - 0.1 s corresponding to a significant decrease of the drop temperature by 30…60 K. This long nucleation interval is caused by two factors: (i) high cooling rates in DTP, and (ii) the finite volume of drops and strong interaction of nuclei via thermal and solute fields.

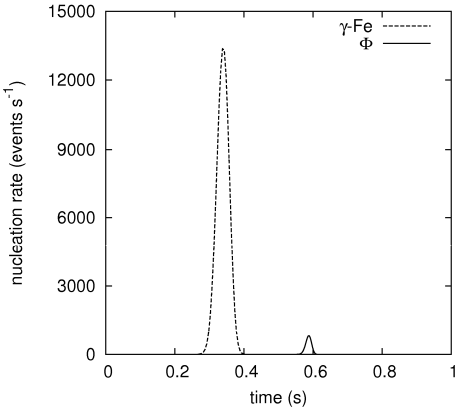

Fig. 9 Nucleation rate of the γ-Fe and Φ phases as a function of time in a 1000 μm diameter drop.

After nucleation, the growth behavior of the γ-Fe and Φ phases are different[15]. Due to high solute rejection, growth velocity of γ-Fe is small. On the other hand, the alloy composition is close to the Φ phase. Therefore, the growth velocity of Φ is large and growth is limited by heat transport (*cf.* Fig. 6). Immediately after nucleation, growth of Φ is controlled by heat diffusion into the melt. After recalescence, growth is limited by heat exchange at the drop surface. Due to the difference in the growth velocities of both phases, the γ-Fe nuclei achieve a dimensionless size of about 5% of the drop radius before nucleation of Φ. The subsequent nucleation of the Φ phase results in fast growth and dominant Φ phase solidification. This is in good agreement with experimental data on DTP of Nd-Fe-B where small drops show bigger volume fractions of Φ[15]. A change from a flow velocity of 10^{-4} in small drops to 10^{-2} m/s in large drops leads to significant increase of the growth velocity of γ-Fe (*cf.* Fig. 6).

Phase selection in Nd-Fe-B is governed by competition between nucleation and diffusion-limited growth which are influenced by convection. From our modeling, we conclude that the transients in the internal flow lead to reduced flow velocity in DTP experiments. Nucleation of γ-Fe is observed at small undercooling while Φ forms as the primary phase at high undercooling. The high cooling rate in DTP suppresses γ-Fe formation and leads to the preferential formation of Φ phase. Therefore, small drops contain a high volume fraction of Φ while large drops exhibit a significant amount of γ-Fe.

5. Summary

Containerless experiments have revealed metastable phase formation in Fe-Co, Fe-Ni undercooled melts. The lifetime of the metastable phase is increased in microgravity. Phase field modeling reflects a transition from the nucleation of the stable *fcc* structure to the metastable *bcc* phase when decreasing the Ni content of the liquid. EML experiments on undercooled Nd-Fe-B melts proved the competition of Φ-$Nd_2Fe_{14}B$ and γ-Fe solidification. A lower flow velocity in the melt, expected under microgravity conditions, can favor the growth of the Φ-phase. Nucleation of γ-Fe is observed at small undercooling while Φ forms as the primary phase at high undercooling. The high cooling rate in DTP suppresses γ-Fe formation and favors Φ formation.

Acknowledgment

This work is financially supported by ESA under AO99-101 ESTEC Contract No. 14980/01/NL/SH, and PECS Contract No. 98059. T.P. is a grantee of the Bolyai János Scolarship.

References

1) Hermann, R., Löser, W., Lindenkreuz, H.-G., Diefenbach, A., Zahnow, W., Dreier, W., Volkmann, T. and Herlach, D.M., *Mater. Sci. Eng. A*, **375-377,** 507, 2004.
2) Eckler, K., Gartner, F., Assadi , H., Norman, A.F., Greer, A.L. and Herlach, D.M., *Mater. Sci. Eng. A*, **226**, 410, 1997.
3) Hanlon, A.B., Matson, D.M. and Hyers, R.W., *Phil. Mag. Lett.*, **86**, 165, 2006.
4) Woodcock, T.G., Hermann, R. and Löser, W., *CALPHAD*, **31,** 256, 2007.
5) Alexander, S. and McTague, J., *Phys. Rev. Lett.*, **41**, 702, 1978; Groh, B. and Mulder, B., *Phys. Rev. E*, **59**, 5613, 1999; Klein, W., *Phys. Rev. E*, **64**, 056110, 2001.
6) ten Wolde, P. R. Ruiz-Montero, M. J. and Frenkel, D., *Phys. Rev. Lett.*, **75**, 2714, 1995.
7) Hoyt, J.J., Asta, M. and Karma, A., *Mater. Sci. Eng. R*, **41**, 121 2003.
8) Lewis, D., Pusztai, T., Gránásy, L., Warren, J. and Boettinger, W., *JOM*, **56**, 34, 2004.
9) Steinbach, I. et al., *Physica D*, **94,** 135, 1996.
10) Gránásy, L., Pusztai, T., *J. Chem. Phys.*, **117**, 10121, 2002.
11) Chuang, Y.Y., Hsiei, K.C., and Chang, Y.A., *Metall. Trans. A*, **17**, 1373, 1986.
12) Gránásy, L., Tegze, M., *Mater. Sci. Forum* **77**, 243, 1991.
13) Sun, D. Y., Asta, M. and Hoyt, J.J., *Phys. Rev. B*, **69**, 174103, 2004.
14) Gao, J., Volkmann, T. and Herlach, D.M., *Acta Mater.*, **50**, 3003, 2002.
15) Gao, J., Volkmann, T., Yang, S., et al., *J. Alloys and Compounds*, **433**, 356, 2007.
16) Krivilyov, M. and Fransaer, J., *Proc. of ICCFD4*, 2006.
17) Fransaer, J., Wagner, A.V., Spaepen, F., *J. Appl. Phys.*, **87**, 1801, 2000.